Correspondence to:
P. Ludwig,
pludwig@meteo.uni koeln.de

Impacts of surface boundary conditions on regional climate model simulations of European climate during the Last Glacial Maximum

Patrick Ludwig[1]   , **Joaquim G. Pinto**[2]   , **Christoph C. Raible**[3,4]   , and **Yaping Shao**[1]

[1]Institute for Geophysics and Meteorology, University of Cologne, Cologne, Germany, [2]Institute of Meteorology and Climate Research, Karlsruhe Institute of Technology, Karlsruhe, Germany, [3]Climate and Environmental Physics, University of Bern, Bern, Switzerland, [4]Oeschger Centre for Climate Change Research, University of Bern, Bern, Switzerland

Abstract We examine the influences of North Atlantic sea surface temperatures (SSTs) and vegetation on regional climate simulations over Europe during the Last Glacial Maximum (LGM). Simulated regional temperature and precipitation patterns over Europe are considerably improved when using revised SSTs based on proxy data. Likewise, the simulated permafrost is more accurately reproduced with the SST modifications. These improvements are partially related to the changed regional atmospheric circulation due to the revised SSTs, leading to colder and drier conditions over Western Europe. Further sensitivity tests with prescribed vegetation for LGM conditions provide evidence of the sensitivity of the simulated glacial climate. This study reveals the importance of considering more realistic SST and vegetation boundary conditions for a more accurate representation of regional climate variability under glacial conditions.

1. Introduction

The Earth's climate of the last million years is characterized by alternations between glacial and interglacial periods. Fundamental drivers of these oscillations are most likely the changes of the Earth's orbital parameters, also known as "Milankovich Cycles" [*Berger et al.*, 1984]. Also, variations in greenhouse gas (e.g., CO_2) concentration are in line with the glacial/interglacial cycles [*Sigman and Boyle*, 2000, Figure 1] and are thus considered as an additional driver of (past) climate changes. The Last Glacial Maximum (LGM) of the last glacial cycle is defined as the time period of global maximum land ice volume (22–19 ka B.P. [*Yokoyama et al.*, 2000]). Proxy data show that the climate in Europe was much colder and drier during the LGM compared to recent climate conditions [e.g., *Bartlein et al.*, 2011; *Annan and Hargreaves*, 2013].

Such different climatic conditions are used to test state-of-the art Earth system models in order to gain confidence in them for future climate projections [*Harrison et al.*, 2016]. Within the framework of the third phase of the Paleoclimate Modelling Intercomparison Project (PMIP3) [*Braconnot et al.*, 2012], steady state time slice experiments for the LGM were performed using coupled general circulation models (CGCMs) to investigate the Earth's climate under glacial conditions. These CGCMs show colder and drier conditions compared to today, though underestimating the amplitudes of the changes compared to proxy evidence. Increasing the horizontal resolution further illustrated that the ice sheet over North America is an important player in determining the atmospheric circulation and the temperature and precipitation distribution over Europe [*Hofer et al.*, 2012a, 2012b; *Merz et al.*, 2015].

PMIP3 CGCMs generally simulate too wet conditions over the Iberian Peninsula compared to proxy data [*Beghin et al.*, 2016; *Ludwig et al.*, 2016]. This bias has been partially attributed to differences in the general atmospheric circulation (e.g., regarding the eddy-driven jet stream and weather-type frequencies [*Ludwig et al.*, 2016]) as well as to a poor representation of glacial ocean conditions in the CGCMs. As shown in *Ludwig et al.* [2016] for some CGCMs, the LGM sea surface temperatures (SSTs) over the North Atlantic were even higher than the preindustrial SSTs, probably due to a too strong Atlantic meridional overturning circulation simulated for the LGM. A comparison of the CGCM SSTs with reconstructions of the Multiproxy Approach for the Reconstruction of the Glacial Ocean surface (MARGO) project [*MARGO Project Members*, 2009] shows that almost all CGCMs (particularly Max-Planck-Institut Earth system model, MPI-ESM) [*Stevens et al.*, 2013] tend to overestimate the SSTs over the northeastern parts of the North Atlantic [*Wang et al.*, 2013, Figure 3b]. This influences the climate over Western Europe (see Figure 1a for MPI-ESM-P model deviations), where the simulated 2 m
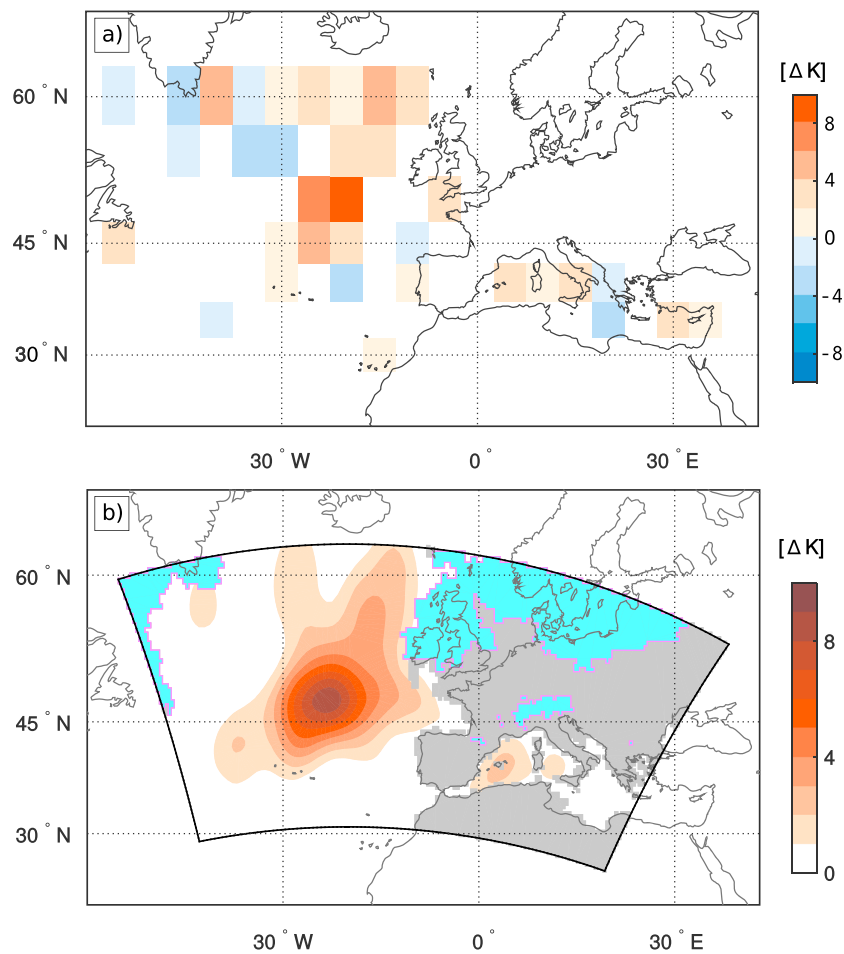
Figure 1. (a) SST differences between MPI LGM simulation and MARGO reconstruction over the North Atlantic. (b) Model domain (black line), extended land area (gray, shaded), ice sheets following PMIP3 protocol and *Ehlers et al.* [2011] (aqua, shaded), and interpolated SST anomalies applied to WRF MARGO.

temperature is too warm during the LGM compared with a reconstructed permafrost border [*Maier et al.*, 2016].

As indicated by *Harrison et al.* [2015], there is evidence of modest overall model skill for the mid-Holocene and LGM and of substantial misrepresentation of past regional climates in the state-of-the-art GCMs. Dynamical downscaling techniques can be helpful to test climate sensitivity and feedback mechanisms on the regional scale and have been widely used for recent, present, and future climate projections [e.g., *Giorgi and Gutowski*, 2015; *Jacob et al.*, 2014]. Regional climate models (RCMs) can both add value to [*Feser et al.*, 2011; *Hackenbruch et al.*, 2016] and reduce the biases in the GCM simulations [*Diaconescu and Laprise*, 2013], as the higher resolution permits a better representation of relevant physical processes for regional weather and climate. So far, RCMs have only been scarcely used for past climate simulations in Europe, e.g., for the Common Era [e.g., *Gomez-Navarro et al.*, 2015; *Raible et al.*, 2017], the Younger Dryas [*Renssen et al.*, 2001], and the LGM [*Strandberg et al.*, 2011]. In this study, the influences of the SSTs in the eastern North Atlantic on the regional LGM climate over Europe are investigated with RCM simulations. Sensitivity simulations are performed with different SST patterns, either based on the original CGCM SSTs or based on SST proxies. The simulations are compared against existing climate proxy data, also with respect to the role of regional circulation patterns. Additionally, the climate sensitivity to glacial vegetation in the RCM is assessed, since vegetation is basically prescribed to preindustrial (PI) conditions in the PMIP3 CGCMs [*Brady et al.*, 2013; *Sueyoshi et al.*, 2013].

2. Model and Data

The MPI-ESM-P (henceforth MPI) simulations are dynamically downscaled with the Weather Research and Forecast model (WRF [*Skamarock et al.*, 2008]). Data from the PMIP3 MPI-PI and MPI-LGM experiments are used to update the atmospheric boundary conditions (6-hourly) and SST and sea ice cover (daily). The final 31 years of the MPI experiments are downscaled. The first year is used as spin-up to guarantee that the land surface processes are almost in equilibrium with the atmosphere and is excluded from further analysis. The WRF model (version 3.5.1) is used with the Polar-WRF extensions (version 3.6 [*Hines et al.*, 2015]) to consider sea ice variability as provided by the driving MPI model. The model domain (Figure 1b) covers the North Atlantic and large parts of Europe with a horizontal resolution of 50 km and 35 layers in the vertical. Physical parameterizations include the Kain-Fritsch convection scheme [*Kain*, 2004], five-class single moment microphysics [*Hong et al.*, 2004], the rapid radiative transfer model for shortwave and longwave radiation [*Iacono et al.*, 2008], the unified Noah Land Surface Model [*Tewari et al.*, 2004], and the Yonsei University boundary layer scheme [*Hong et al.*, 2006]. These parameterizations are different to those used in the CGCMs but are well tested for higher resolution and thus potentially one of the reasons for reducing the CGCM biases.

For glacial simulations, the greenhouse gas concentrations, orbital parameters, lowered sea level, and increased ice sheets are used as specified in the PMIP3 protocol. Additional areas with glaciation (e.g., Alps and Pyrenees) are obtained from *Ehlers et al.* [2011]. Land use and vegetation are initially set to present-day conditions to ensure that differences in the LGM experiments are restricted to changes in SSTs.

Four simulations were performed to analyze the influence of altered glacial SSTs on the European climate during the LGM. A control simulation forced by the PI conditions (henceforth WRF-PI) is used as reference to determine changes between the (recent past) control climate and the LGM forced simulation (WRF-LGM). The annual mean SST differences over the eastern North Atlantic and the Mediterranean (from MARGO; Figure 1b) are taken into account together with the corresponding sea ice changes (ocean grid points are considered as sea ice if SST $<$ 271.15 K at each input time step) to study the influence of revised SSTs on the European glacial climate (WRF-MARGO). To focus on the influence of warm SSTs, only positive deviations over the eastern North Atlantic are interpolated to the WRF grid. Finally, the sensitivity to changes in vegetation cover and land use as obtained from the Climate: Long-range Investigation, Mapping, and Prediction (CLIMAP) data set [*CLIMAP Project Members*, 1984] is assessed (WRF-CLIMAP). Here we use the same atmospheric and oceanic boundary conditions as in WRF-MARGO, but with LGM-like vegetation cover and land use types (see Figure S2 and Table S1 in the supporting information). Gridded temperature and precipitation proxy data [*Bartlein et al.*, 2011] are used for comparison with the model output. With this aim, the WRF data are interpolated onto the 2° proxy data grid, which includes 13 proxy sites within the domain.

Permafrost distribution is calculated using the surface frost index (SFI) [*Nelson and Outcalt*, 1987]. The index (SFI $= \sqrt{\mathrm{DDF}}/(\sqrt{\mathrm{DDF}} + \sqrt{\mathrm{DDT}})$) uses the sum of annual freezing (thawing) degree-days DDF (DDT), which is the sum of daily temperatures below (above) 0°C. Here simulated WRF or MPI soil temperatures are used to calculate the SFI. Considering soil temperatures allows a direct SFI calculation without special treatment of insolation effects due to snow cover [cf. *Stendel and Christensen*, 2002]. An SFI between 0.5 and 0.67 defines areas with sporadic and discontinuous permafrost; an SFI above 0.67 is taken as continuous permafrost. The reconstructed LGM permafrost distribution over Central Europe is obtained from *Baulin et al.* [1992] and is compared to the different simulations.

Circulation weather types (CWTs), which characterize the regional atmospheric circulation over a given area [*Jones et al.*, 1993], are calculated based on daily mean sea level pressure. For comparison between WRF and MPI-ESM, CWT frequencies obtained by *Ludwig et al.* [2016] are used.

3. Results

The simulations testing the sensitivity to North Atlantic SSTs are first compared to proxy data focusing on the 2 m temperature and precipitation in Europe, followed by the evaluation of the simulated permafrost extension with respect to proxy data. To gain additional insight into the underlying mechanisms of how the SSTs influence the temperature and precipitation patterns, the response of atmospheric circulation to SST changes
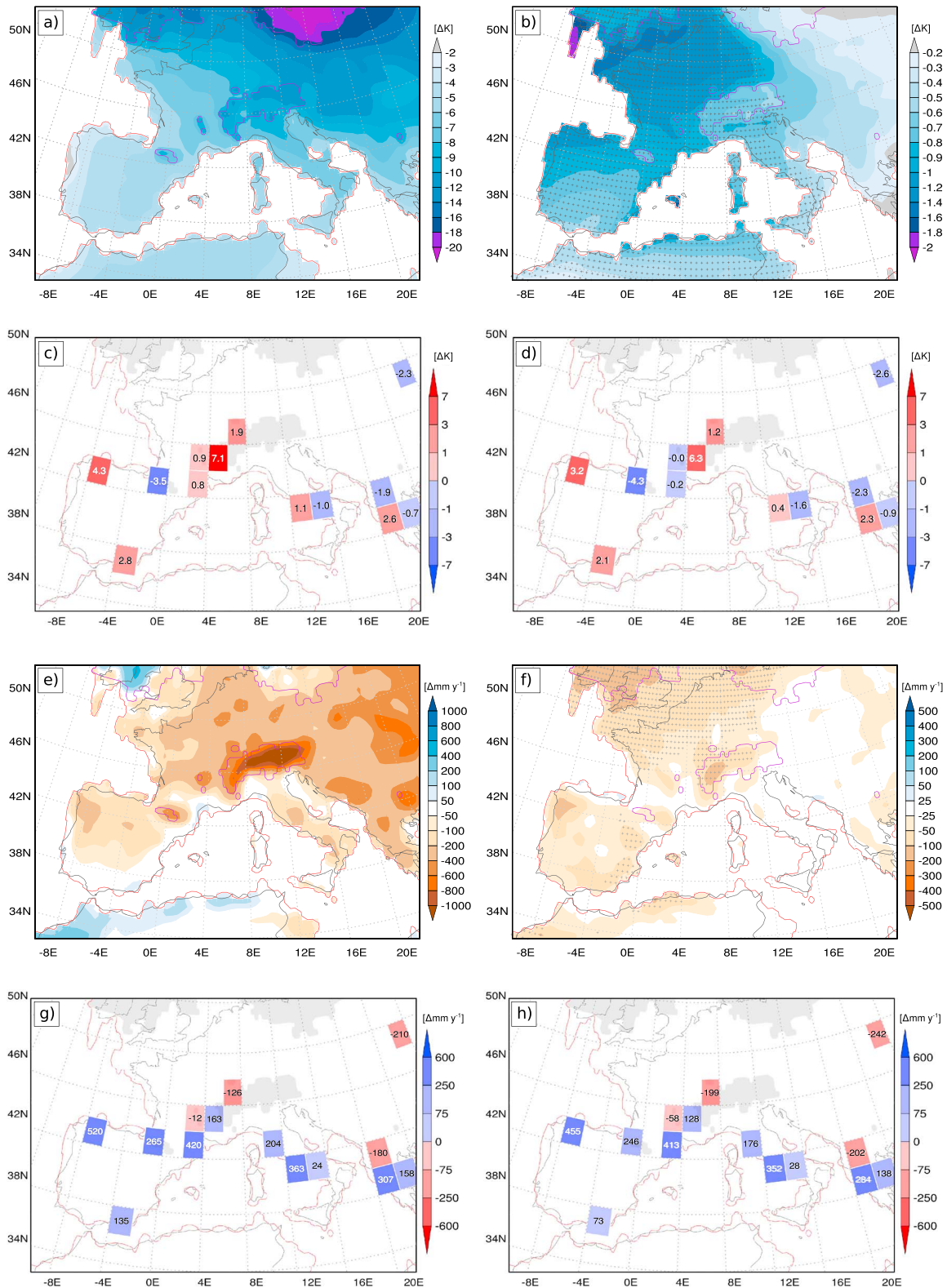
Figure 2. Results of WRF simulations and comparison to reconstructed temperature/precipitation data [*Bartlein et al.*, 2011]: (a) temperature change (K) between WRF LGM and WRF PI; significant changes (two sided Student's *t* test, 90% confidence interval) at almost all grid points, not depicted. (b) Temperature change (K) between WRF MARGO and WRF LGM (note different color scaling; significant changes are indicated by the plus symbol). (c) Difference of temperature changes as reconstructed by Bartlein and from WRF LGM and WRF PI. (d) Same as in Figure 2c but for WRF MARGO and WRF PI. (e g) Same as in Figures 2a 2d but for precipitation. Gray shades/purple line: LGM ice sheet, red line: LGM coastline.
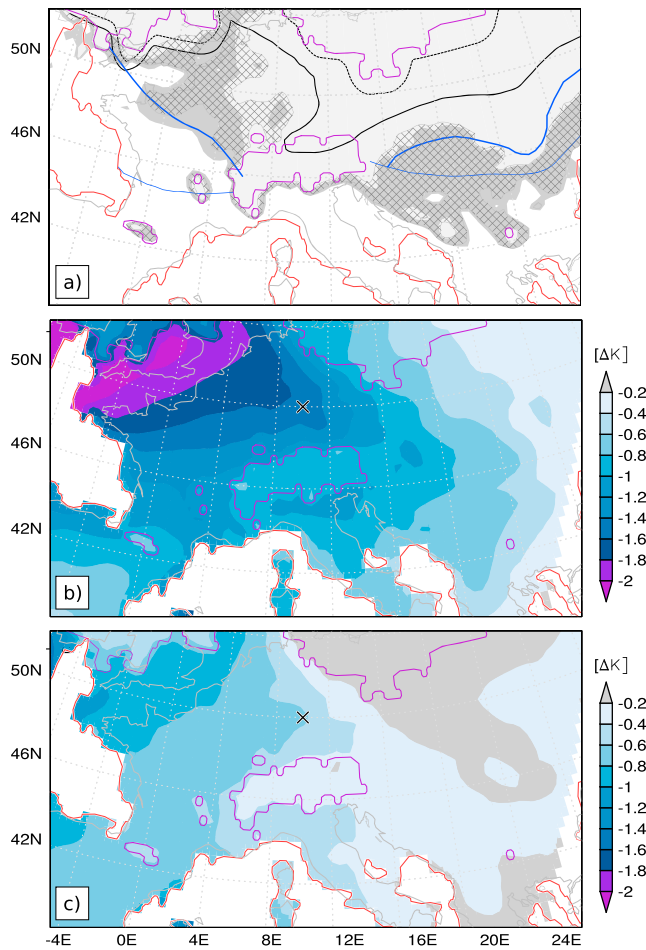
Figure 3. (a) Distribution of sporadic (thin blue line) and continuous (bold blue line) permafrost during LGM after *Baulin et al.* [1992]. Black line: sporadic and continuous permafrost based on SFI (0.5: solid, 0.67: stippled) from MPI data. Gray shades: SFI (0.5: dark gray, 0.67: light gray) for WRF MARGO. Hatching indicates the area of sporadic and discontinuous permafrost covered by SFI values between 0.5 and 0.67 for WRF LGM. (b) Temperature difference (K) between WRF MARGO and WRF LGM for maritime weather types (S, SW, W, and NW). (c) Same as in Figure 3b but for continental weather types (N, NE, E, and SE). Purple line: LGM ice sheet, red line: LGM coastline.

is discussed. Finally, the sensitivity of the simulated climate to the LGM-like vegetation and land use types is analyzed.

3.1. Temperatures and Precipitation

The comparison of the RCM output with the proxy data shows a better agreement of the regional WRF-LGM than the global MPI-LGM simulation (Figure S1). The overall significant (confidence interval 90%) cooling over Europe during the LGM (Figure 2a) is more appropriate in the regional WRF-LGM simulation (Figure 2c). While the mean deviation at the considered proxy locations shows a warm bias of 2.44 K for MPI-LGM, it is reduced to 0.93 K in WRF-LGM. Still, obvious differences between simulation and proxies are found, particularly over Western Europe (Figure 2c). A comparison of WRF-MARGO and WRF-PI shows a reduction of the warm bias to 0.28 K at the proxy locations (Figure 2d). Reduced SSTs over the North Atlantic and Mediterranean in WRF-MARGO cause a further temperature decrease of 1–1.4 K over Western Europe and an attenuated decrease of 0.2–0.6 K farther east (Figure 2b).

The reduced SSTs over the North Atlantic also affect the precipitation patterns. A general (significant; confidence interval 90%) decrease of precipitation is observed in WRF-LGM, with a gradient from a moderate decrease in the western to a strong decrease in the eastern parts of the domain (Figure 2e). While the MPI strongly underestimates the decrease of precipitation during the LGM over Europe (Figure S1d) on average by 335 mm, the bias is reduced to 145 mm in WRF-LGM and 113 mm in WRF-MARGO. Both WRF-LGM and MPI-LGM show strongest precipitation deviations from proxy data over the northern parts of the Iberian Peninsula (IP; Figure 2g). In WRF-MARGO, precipitation is decreased particularly over the IP and significantly (confidence interval 90%) to the south of the western parts of the Fennoscandian ice sheet (Figure 2f) as compared to WRF-LGM. This leads to a reduced precipitation difference of, e.g., 65 mm yr^{-1} (12%, northwestern Iberia) and 63 mm yr^{-1} (46%, Andalusia), between WRF-LGM and WRF-MARGO and thus a better representation of mean temperature and precipitation compared to proxy data.

3.2. Permafrost Distribution

As shown in Figure 3a, the MPI failed to reproduce the permafrost distribution over Central Europe. Areas with SFI > 0.67 are restricted to the Fennoscandian ice sheet. The area featuring sporadic and

discontinuous permafrost reaches farther south but is still north to the reconstructed continuous permafrost line after *Baulin et al.* [1992] (Figure 3a). The permafrost distribution for WRF-MARGO is in much better agreement with the reconstructed permafrost distribution, particularly east of the Alps where observed and simulated continuous permafrost overlap reasonably well. Still, the simulated continuous permafrost border over Western Europe is displaced toward the east, located at around 5°E. Nevertheless, WRF-MARGO exhibits an enhanced area of continuous permafrost by 0.2 mio km^2 over the domain compared to the continuous permafrost given by WRF-LGM. The sporadic and discontinuous permafrost distribution over Eastern Europe is similar for both WRF simulations, exhibiting a too far southward extension of the area covered by sporadic permafrost compared to *Baulin et al.* [1992]. For Western Europe, the area of sporadic and discontinuous permafrost is located farther west in WRF-MARGO, reaching the extension of the continuous permafrost distribution after *Baulin et al.* [1992]. Thus, the area of sporadic permafrost is still not well reproduced by WRF-MARGO, with too warm conditions over western parts of Europe remaining.

3.3. Atmospheric Circulation

The regional atmospheric circulation is characterized based on CWTs. A comparison of the CWTs for PI conditions between WRF and MPI-ESM (Tables S2 and S3) shows improved RCM-modeled CWT frequencies compared with those based on National Centers for Environmental Prediction reanalysis [*Kalnay et al.*, 2006]. In particular, the under- (over-) representation of the anticyclonic (western) CWT in MPI-PI is adjusted in the WRF-PI simulation (Table S3). The CWT distributions for WRF-LGM and WRF-MARGO are similar, indicating that weather pattern frequencies remain almost unchanged by the modified SSTs.

To illustrate the influence of the reduced SSTs on the Central European temperature distribution, we compared the alterations of the 2 m temperature depending on the prevailing atmospheric CWTs. Figure 3b shows the temperature difference of the maritime characterized CWTs (northwest, west, southwest, and south) in comparison to the more continental characterized CWTs (north, northeast, east, and southeast) between WRF-MARGO and WRF-LGM. The maritime CWTs (Figure 3b) feature a stronger temperature decrease particularly over Western Europe compared to the continental CWTs (Figure 3c). Additionally, the temperature decrease propagates farther east in the WRF-MARGO simulation for the maritime CWTs.

The Central European temperature differences are considerably influenced by reduced SSTs particularly for individual maritime CWTs (Figure S3). The same is found for the precipitation differences between WRF-MARGO and WRF-LGM of some CWTs, where the largest precipitation differences over Central Europe are again associated with maritime CWTs (Figure S4). Additionally, the southeastern CWT exhibits a decrease of precipitation over western parts of Central Europe due to less moisture advection from the (artificially cooled) Mediterranean in WRF-MARGO. Strongest precipitation decrease occurs along the southern boundary of the Fennoscandian ice sheet for southern to western CWTs. Here the orographically induced rainfall is weakened due to reduced moisture advection. A considerable reduction of precipitation also occurs for the cyclonic CWT, which is associated with low-pressure areas approaching Central Europe carrying comparatively less moisture from the cooler North Atlantic.

We additionally analyze the WRF-MARGO and WRF-LGM differences for the IP based on the CWT distribution for Western Europe (Table S3). The eastern CWTs have only little effect on the 2 m temperature differences over the IP, except a moderate influence along the east coast (Figure S5). The western and cyclonic WRF-MARGO CWTs provide a stronger temperature decrease particularly over the northwestern parts of the IP that are exposed to moisture advection from the area of reduced SSTs over the North Atlantic. For precipitation, the eastern CWTs show a decrease in (south-) eastern parts of the IP (Figure S6), which is related to the reduced evaporation over the Mediterranean (about 1 mm d^{-1}; not shown). The northwestern, northern, and particularly cyclonic CWTs, advecting less moisture from the cooled North Atlantic, lead to decreased precipitation particularly in northwestern Spain. The slight increase of precipitation associated with the southwestern and western CWTs is related to slightly increased evaporation over the North Atlantic south to the area with reduced SSTs (around 40°N).

In summary, our results suggest that the distinct influence of the reduced SSTs on temperature and precipitation over Europe is associated with changes in CWT characteristics. Thus, changes in the atmospheric circulation play an important role in explaining the temperature and precipitation differences identified in the sensitivity simulations.
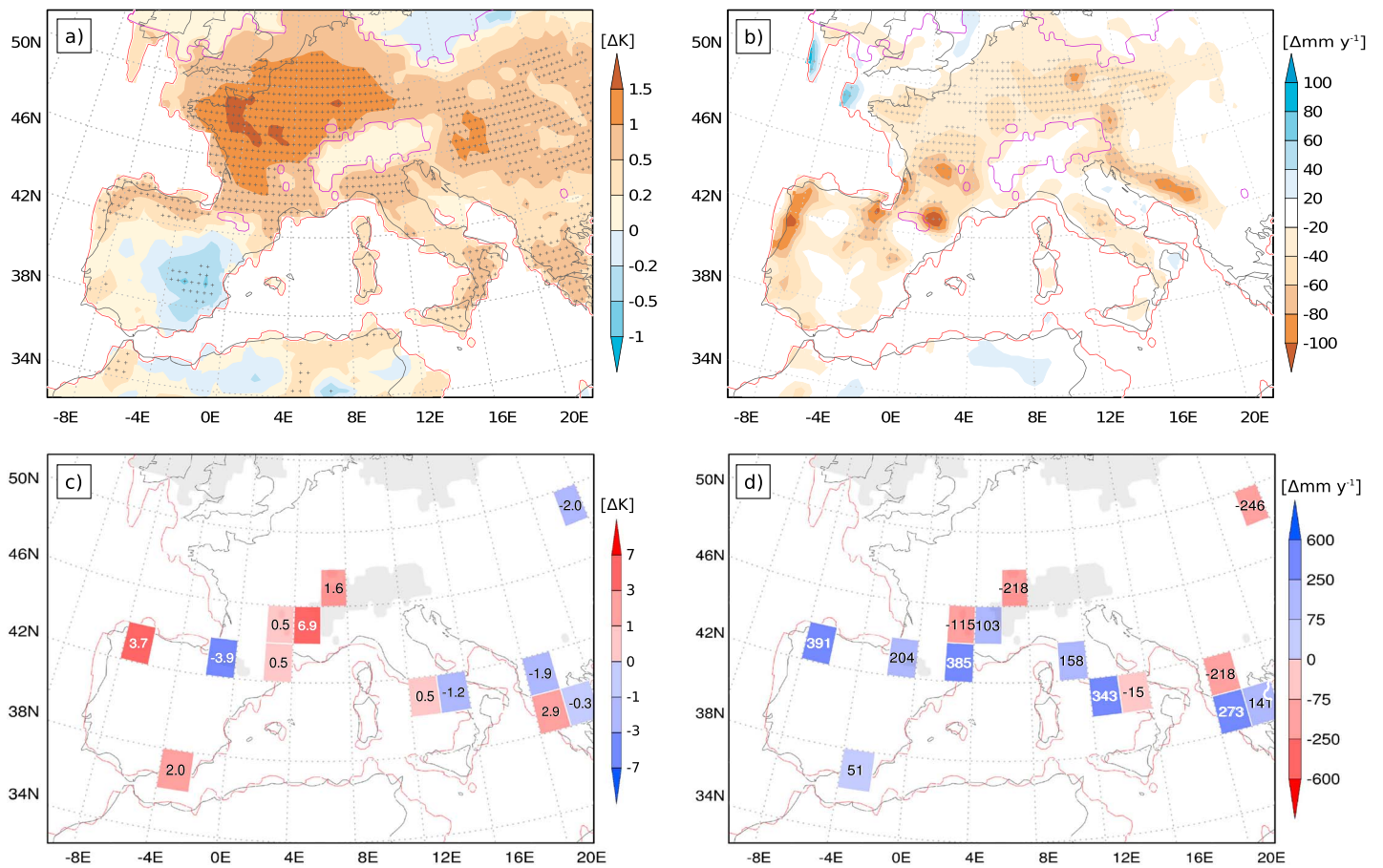
Figure 4. (a) Annual mean temperature (K) and (b) precipitation (mm yr^{-1}) changes between WRF CLIMAP and WRF MARGO. Significant changes (two sided Student's *t* test, 90% confidence interval) indicated by the plus symbol. (c) Differences of temperature changes as reconstructed by *Bartlein et al.* [2011] and from WRF CLIMAP and WRF PI. (d) Same as in Figure 4c but for precipitation. Red line: LGM coastline, dashed black line: LGM ice sheet.

3.4. Sensitivity to Prescribed Glacial Vegetation

The response of the changed vegetation on temperature and precipitation is rather different compared to the SST sensitivity simulations (Figure 4). WRF-CLIMAP exhibits warmer temperatures over most parts of Europe compared to WRF-MARGO, except for the eastern part of the IP. The modification of the land use types affects the net radiation, latent and sensible heat fluxes, and the surface albedo. While the (present day) land use over Central Europe used in WRF-MARGO is dominated by cropland (albedo 0.17–0.23), the dominant WRF-CLIMAP land use is herbaceous tundra (albedo 0.15–0.2; Figure S2). During winter, Central Europe was covered by snow; thus, the lower albedo in WRF-CLIMAP leads to higher temperatures, especially during summer, resulting in slightly higher annual mean temperatures (1–1.5 K) over western parts of Central Europe. Accordingly, the net radiation as well as the surface heat flux exhibits increased values for WRF-CLIMAP (not shown). For the IP, land use in WRF-CLIMAP is dominated by shrubland (albedo 0.25–0.3) compared to the dominant cropland land use types in WRF-MARGO (albedo 0.17–0.23), leading to slightly lower temperatures in WRF-CLIMAP. Eventually, this leads to a weaker temperature decrease as in WRF-MARGO and thus a warm bias of 0.72 K (0.28 K for WRF-LGM) over Europe compared to *Bartlein et al.* [2011] proxy data. Our results are in contrast to a modeling study by *Strandberg et al.* [2011], where the authors showed that March temperatures (when vegetation differences are pronounced) decrease by about 1–3 K, assuming glacial vegetation. For Central Europe, they assumed potential vegetation dominated by deciduous forest for present days (in contrast to cropland in our case), having lower albedo than their glacial herbaceous vegetation. Based on *Kaplan et al.* [2011], Central Europe had already lost a large amount of its natural vegetation due to anthropogenic land cover change by 1850 (the representative year for PI conditions). Thus, a combination of cropland and natural vegetation potentially describes best the PI land use.

For precipitation, generally drier conditions were simulated for WRF-CLIMAP compared to WRF-MARGO. The wet bias compared to *Bartlein et al.* [2011] data is further reduced to 89 mm yr^{-1} (267 mm yr^{-1} versus 356 mm yr^{-1} in WRF-MARGO, corresponding to a relative change of 22%). The changed land use types (mainly cropland versus sparsely vegetated herbaceous tundra; Figure S2) and vegetation cover cause less evapotranspiration (not shown [e.g., *Liu et al.*, 2003, Table 2]) as simulated by the NOAH land surface model resulting in reduced water recycling that leads to less precipitation.

4. Summary and Discussion

The influences of North Atlantic SSTs and vegetation on simulations of the European climate during the LGM are investigated in a set of sensitivity experiments using a regional climate model. The results of the sensitivity simulations are in better agreement with reconstructed 2 m temperature, precipitation, and permafrost over Europe [*Bartlein et al.*, 2011; *Baulin et al.*, 1992] when using proxy-based SSTs over the North Atlantic and LGM-like reconstructions for vegetation [*CLIMAP Project Members*, 1984]. Thereby, the impact of SSTs on the CWTs over Europe [*Ludwig et al.*, 2016] is important. Since the majority of PMIP3 CGCMs overestimate North Atlantic SSTs, our findings for SST-climate feedbacks in Europe under glacial conditions may be generalized to other simulations with similar biases.

Still, some biases remain. Including LGM-like vegetation distribution in the model leads to a slightly increase of the warm bias due to higher albedo, changes in the net radiation, and sensible and latent heat fluxes. However, *Jahn et al.* [2005] quantified the global temperature decrease-based vegetation cover changes to be 0.6 K during the LGM, providing a hint of the uncertainties associated with the LGM vegetation reconstructions of *CLIMAP Project Members* [1984]. In contrast to temperature, precipitation improves considerably, reducing the wet bias to 89 mm. An additional comparison with seasonal proxy data (mean temperature of the coldest/warmest month, MTCO/MTWA; Figure S7 and Table S6) reveals a good agreement of the model results for MTWA but a strongly underestimated decrease for MTCO by both MPI-ESM and WRF. This behavior opposes another modeling study for the LGM with a different CGCM [*Hofer et al.*, 2012b], who found a better agreement during MTCO than MTWA when comparing with the proxy data of *Wu et al.* [2007]. Still, proxies might be more sensitive to climatic extremes than to the average climate values, which may lead to large discrepancies of climate variables during glacial conditions [*Kageyama et al.*, 2006]. This is in particular true during the LGM, where the proxy data themselves are associated to high uncertainties [e.g., *Wu et al.*, 2007].

In summary, our study provided evidence that regional paleoclimate simulations lead both to improved patterns for temperature, precipitation (see also Figures S9 and S10), and permafrost, as well as to an improved representation of the regional circulation (CWT analysis). This is in line with *Harrison et al.* [2015], who called for improvements to generate reliable regional projections. An additional GCM experiment with MARGO SSTs would enable to test if similar improvements for temperature and precipitation could be achieved with a GCM. Nevertheless, the more realistic distributions of temperature and precipitation by the RCM (Figures S9 and S10) clearly reflect the added value of using a high-resolution regional climate model. Our results demonstrate the climate sensitivity to revised SSTs over the North Atlantic Ocean and to changes in boundary conditions as land use and vegetation under glacial conditions, where the latter is hypothesized to be also influenced by human activity [*Kaplan et al.*, 2016]. Thus, a realistic representation of glacial boundary conditions (SSTs and vegetation) is essential to obtain a more accurate representation of the regional (paleo-) climate.

References

Annan, J. D., and J. C. Hargreaves (2013), A new global reconstruction of temperature changes at the Last Glacial Maximum, *Clim. Past*, 9, 367 376, doi:10.5194/cp 9 367 2013.

Bartlein, P. J., et al. (2011), Pollen based continental climate reconstructions at 6 and 21 ka: A global synthesis, *Clim. Dyn.*, 37, 775 802.

Baulin, V. V., N. S. Danilova, V. P. Nechayev, T. L. Pewe, and A. A. Velichko (1992), Permafrost: Maximum cooling of the last glaciation (about 20,000 to 18,000 yr B.P.), in *Atlas of Paleoclimates and Paleoenvironments of the Northern Hemisphere*, edited by B. Frenzel, M. Pecsi, and A. A. Velichko, pp. 49 50, Geographical Research Institute, Hungarian Academy of Sciences, Budapest, Gustav Fischer Verlag, Stuttgart.

Beghin, P., S. Charbit, M. Kageyama, N. Combourieu Nebout, C. Hatte, C. Dumas, and J. Y. Peterschmitt (2016), What drives LGM precipitation over the western Mediterranean? A study focused on the Iberian Peninsula and northern Morocco, *Clim. Dyn.*, 46, 2611 2631.

Berger, A., J. Imbrie, J. Hays, G. Kukla, and B. Saltzman (Eds.) (1984), *Milankovitch and Climate*, pp. 269 305, D. Reidel, Boston.

Braconnot, et al. (2012), Evaluation of climate models using palaeoclimatic data, *Nat. Clim. Change*, 2, 417 424, doi:10.1038/nclimate1456.

Brady, E. C., B. L. Otto Bliesner, J. E. Kay, and N. Rosenbloom (2013), Sensitivity to glacial forcing in the CCSM4, *J. Clim.*, *26*, 1901 1925.

CLIMAP Project Members (1984), The last interglacial ocean, *Quat. Res.*, *2*, 123 224, doi:10.1016/0033 5894(84)90098 X.

Diaconescu, E. P., and R. Laprise (2013), Can added value be expected in RCM simulated large scales?, *Clim. Dyn.*, *41*, 1769.

Ehlers, J., P. L. Gibbard, and P. D. Hughes (Eds.) (2011), *Quaternary Glaciations Extent and Chronology: A Closer Look*, p. 1126, Elsevier, Amsterdam.

Feser, F., B. Rockel, H. von Storch, J. Winterfeldt, and M. Zahn (2011), Regional climate models add value to global model data: A review and selected examples, *Bull. Am. Meteorol. Soc.*, *92*, 1181 1192.

Giorgi, F., and W. J. Gutowski Jr. (2015), Regional dynamical downscaling and the CORDEX initiative, *Annu. Rev. Environ. Resour.*, *40*, 467 490.

Gomez Navarro, J. J., O. Boethe, S. Wagner, E. Zorita, J. P. Werner, J. Luterbacher, C. C. Raible, and J. P. Montavez (2015), A regional climate palaeosimulation for Europe in the period 1501 1990. Part II: Comparison with gridded reconstructions, *Clim. Past*, *11*, 1077 1095.

Hackenbruch, J., G. Schädler, and J. W. Schipper (2016), Added value of high resolution regional climate simulations for regional impact studies, *Meteorol. Z.*, *25*, 291 304, doi:10.1127/metz/2016/0701.

Harrison, S. P., P. J. Bartlein, K. Izumi, G. Li, J. Annan, J. Hargreaves, P. Braconnot, and M. Kageyama (2015), Evaluation of CMIP5 palaeo simulations to improve climate projections, *Nat. Clim. Chang.*, *5*, 735 743, doi:10.1038/nclimate2649.

Harrison, S. P., P. J. Bartlein, and I. C. Prentice (2016), What have we learnt from palaeoclimate simulations?, *J. Quat. Sci.*, *31*, 363 385, doi:10.1002/jqs.2842.

Hines, K. M., D. H. Bromwich, L. Bai, C. M. Bitz, J. G. Powers, and K. W. Manning (2015), Sea ice enhancements to Polar WRF, *Mon. Weather Rev.*, *143*, 2363 2385, doi:10.1175/MWR D 14 00344.1.

Hofer, D., C. C. Raible, N. Merz, A. Dehnert, and J. Kuhlemann (2012a), Simulated winter circulation types in the North Atlantic and European region for preindustrial and glacial conditions, *Geophys. Res. Lett.*, *39*, L15805, doi:10.1029/2012GL052296.

Hofer, D., C. C. Raible, A. Dehnert, and J. Kuhlemann (2012b), The impact of different glacial boundary conditions on atmospheric dynamics and precipitation in the North Atlantic region, *Clim. Past*, *8*, 935 949.

Hong, S. Y., J. Dudhia, and S. H. Chen (2004), A revised approach to ice microphysical processes for the bulk parameterization of clouds and precipitation, *Mon. Weather Rev.*, *132*, 103 120.

Hong, S. Y., Y. Noh, and J. Dudhia (2006), A new vertical diffusion package with an explicit treatment of entrainment processes, *Mon. Weather Rev.*, *134*, 2318 2341.

Iacono, M. J., J. S. Delamere, E. J. Mlawer, M. W. Shephard, S. A. Clough, and W. Collins (2008), Radiative forcing by long lived greenhouse gases: Calculations with the AER radiative transfer models, *J. Geophys. Res.*, *113*, D13103, doi:10.1029/2008JD009944.

Jacob, D., et al. (2014), Euro CORDEX: New high resolution climate change projections for European impact research, *Reg. Environ. Chang.*, *14*(2), 563 578.

Jahn, A., M. Claussen, A. Ganopolski, and V. Brovkin (2005), Quantifying the effect of vegetation dynamics on the climate of the Last Glacial Maximum, *Clim. Past*, *1*, 1 7, doi:10.5194/cp 1 1 2005.

Jones, P. D., M. Hulme, and K. R. Briffa (1993), A comparison of lamb circulation types with an objective classification scheme, *Int. J. Climatol.*, *13*, 655 663.

Kain, J. S. (2004), The Kain Fritsch convective parameterization: An update, *J. Appl. Meteorol.*, *43*, 170 181.

Kageyama, M., et al. (2006), Last Glacial Maximum temperatures over the North Atlantic, Europe and western Siberia: A comparison between PMIP models, MARGO sea surface temperatures and pollen based reconstructions, *Quat. Sci. Rev.*, *25*, 2082 2102.

Kalnay, E., et al. (2006), The NCEP/NCAR 40 year reanalysis project, *Bull. Am. Meteorol. Soc.*, *77*, 437 471.

Kaplan, J. O., K. M. Krumhardt, E. C. Ellis, W. F. Ruddiman, C. Lemmen, and K. K. Goldewijk (2011), Holocene carbon emissions as a result of anthropogenic land cover change, *The Holocene*, *21*, 775 791.

Kaplan, J. O., M. Pfeiffer, J. C. A. Kolen, and B. A. S. Davis (2016), Large scale anthropogenic reduction of forest cover in Last Glacial Maximum Europe, *PLoS One*, *11*, e0166726, doi:10.1371/journal.pone.0166726.

Liu, J., J. M. Chen, and J. Cihlar (2003), Mapping evapotranspiration based on remote sensing: An application to Canada's landmass, *Water Resour. Res.*, *39*(7), 1189, doi:10.1029/2002WR001680.

Ludwig, P., E. J. Schaffernicht, Y. Shao, and J. G. Pinto (2016), Regional atmospheric circulation over Europe during the Last Glacial Maximum and its links to precipitation, *J. Geophys. Res. Atmos.*, *121*, 2130 2145, doi:10.1002/2015JD024444.

Maier, A., F. Lehmkuhl, P. Ludwig, M. Melles, I. Schmidt, Y. Shao, C. Zeeden, and A. Zimmermann (2016), Demographic estimates of hunter gatherers during the Last Glacial Maximum in Europe against the background of palaeoenvironmental data, *Quat. Int.*, *425*, 49 61, doi:10.1016/j.quaint.2016.04.009.

MARGO Project Members (2009), Constraints on the magnitude and patterns of ocean cooling at the Last Glacial Maximum, *Nat. Geosci.*, *2*, 127 132, doi:10.1038/ngeo411.

Merz, N., C. C. Raible, and T. Woollings (2015), North Atlantic eddy driven jet in interglacial and glacial winter climates, *J. Clim.*, *28*, 3977 3997.

Nelson, F. E., and S. I. Outcalt (1987), A computational method for prediction and regionalization of permafrost, *Arct. Alp. Res.*, *19*, 279 288.

Raible, C. C., O. Baerenbold, and J. J. Gomez Navarro (2017), Drought indices revisited Improving and testing of drought indices in a simulation of the last two millennia for Europe, *Tellus*, *69*, 1296226, doi:10.1080/16000870.2017.1296226.

Renssen, H., R. F. B. Isarin, D. Jacob, R. Podzun, and J. Vandenberghe (2001), Simulation of the Younger Dryas climate in Europe using a regional climate model nested in an AGCM: Preliminary results, *Global Planet. Change*, *30*, 41 57, doi:10.1016/S0921 8181(01) 00076 5.

Sigman, D. M., and E. A. Boyle (2000), Glacial/interglacial variations in atmospheric carbon dioxide, *Nature*, *407*, 859 869.

Skamarock, W. C., J. B. Klemp, J. Dudhia, D. O. Gill, D. M. Barker, M. G. Duda, X. Y. Huang, W. Wang, and J. G. Powers (2008), A description of the advanced research WRF version 3, *NCAR Tech. Note NCAR/TN 475+STR*, 113 pp., doi:10.5065/D68S4MVH.

Stendel, M., and J. Christensen (2002), Impact of global warming on permafrost conditions in a coupled GCM, *Geophys. Res. Lett.*, *29*(13), 1632, doi:10.1029/2001GL014345.

Strandberg, G., J. Brandefelt, E. Kjellström, and B. Smith (2011), High resolution regional simulation of Last Glacial Maximum climate in Europe, *Tellus, Ser. A*, *63*, 107 125, doi:10.1111/j.1600 0870.2010.00485.x.

Stevens, B., et al. (2013), Atmospheric component of the MPI M Earth system model: ECHAM6, *J. Adv. Model. Earth Syst.*, *5*, 146 172, doi:10.1002/jame.20015.

Sueyoshi, T., et al. (2013), Set up of the PMIP3 paleoclimate experiments conducted using an Earth system model, MIROC ESM, *Geosci. Model Dev.*, *6*, 819 836.

Tewari, M., F. Chen, W. Wang, J. Dudhia, M. A. LeMone, K. Mitchell, M. Ek, G. Gayno, J. Wegiel, and R. H. Cuenca (2004), Implementation and verification of the unified NOAH land surface model in the WRF model, 20th conference on weather analysis and forecasting/16th con ference on numerical weather prediction, pp. 11 15.

Wang, T., Y. Liu, and W. Huang (2013), Last Glacial Maximum sea surface temperatures: A model data comparison, *Atmos. Oceanic Sci. Lett.*, *6*, 233 239, doi:10.3878/j.issn.1674 2834.13.0019.

Wu, H. B., J. L. Guiot, S. Brewer, and Z. T. Guo (2007), Climatic changes in Eurasia and Africa at the Last Glacial Maximum and mid Holocene: Reconstruction from pollen data using inverse vegetation modelling, *Clim. Dyn.*, *29*, 211 229, doi:10.1007/s00382 007 0231 3.

Yokoyama, Y., K. Lambeck, P. P. J. De Deckker, and L. K. Fifield (2000), Timing of the Last Glacial maximum from observed sea level minima, *Nature*, *406*, 713 716.

Repository KITopen

Dies ist ein Postprint/begutachtetes Manuskript.